UNIVERSITÀ DEGLI STUDI DI PADOVA

Dipartimento di Fisica e Astronomia

Corso di Laurea Triennale in Fisica

Tesi di Laurea

Spectral analysis and variability of blazar 1ES 1218+304 with the Fermi Large Area Telescope

Relatore

prof. Riccarco Rando

Laureando

Killa Santer

Matricola 1237641

Anno Accademico 2022/2023

Abstract

Blazars are a particular class of Active Galactic Nuclei (AGNs) dominated by a highly variable component of non-thermal radiation produced in relativistic jets close to the line of sight. They exhibit huge apparent luminosities (up to 10^{49} erg/s), irregular and rapid variable emission, strong optical and radio polarization, often superluminal motion and an overall spectrum which can extend from radio to TeV energies. Inside the blazar class, the small sub-sample of Very High Energy (VHE) blazars, i.e. those that are detected in the VHE range (GeV-TeV), is particularly interesting. Several of this observed by the Large Area Telescope (LAT), the primary instrument on the Fermi Gamma-ray Space Telescope mission (which is designed to study the γ-ray range, from $\sim$ 100 MeV to $\sim$ 300 GeV) as well as by Cherenkov detectors, a class of ground-based instruments operating up to $\sim$100TeV.

In this thesis we analyze 10 years of Fermi LAT observation data of the source 1ES 1218+304. In chapter 1, we present the AGN and blazar phenomena. In chapter 2, we introduce the LAT instrument and its main characteristics. Chapter 3 deals with the analysis method (i.e. the maximum likelihood) that we have used to study the blazar SEDs. Analysis results are shown in chapter 4, where some corrections have been applied to take into account the effects of the Extra-galactic Background Light, allowing a comparison with the data relative to the VERITAS Cherenkov Telescope observations.

Contents

List of Figures

List of Tables

Chapter 1

Active Galactic Nuclei (AGNs)

Active Galactic Nuclei, or AGNs, are a subclass of active galaxies, i.e. galaxies that are far brighter than the sum of the emissions by the stellar population alone. In AGNs, a small compact region at the centre, emits non thermal radiation across the entire electromagnetic spectrum, from radio waves to γ rays.

1.1 AGNs structure

In the commonly accepted model an active galactic nucleus consists of a supermassive central black hole (10^6 - 10^8 solar masses) that attracts all the nearby matter forming an accretion disk that is responsible for the high energy emission. In fact AGNs luminosity is bigger than the one of the brightest galaxies and this property cannot be explained with nuclear fusion processes that are associated with stars, but with a more efficient mechanism to produce energy: accretion onto compact objects, in which part of the acquired mass energy can be released in the form of electromagnetic energy. The efficiency of this process far surpasses nuclear fusion, thus explaining the high luminosities: 10% of the total captured mass is converted to energy, while nuclear fusion reaches approximately the $\sim 0.7\%$. For this reason AGNs are observed to outshine all the billions of stars in the galaxy itself.
The accretion disk is surrounded by orbiting gas clouds that are ionized by the accretion disk radiation and produce strong emission lines that are very intense in the visible and UV band, defining the so called *broad line region* or BLR, clouds located here move fast and are very dense. The BLR can be obscured by a torus (or warped disk) made up by dust molecules, whose existence has been revealed by the study of the emission lines. Narrow emission lines are instead produced in the Narrow Line Region (NLR), located beyond the torus, where there are gas clouds with lower densities and smaller velocities.

1.2 AGN's spectrum

The nature of AGNs implies a number of fascinating properties, which include very high luminosities, small emitting regions in most bands (of the order of a mil-

liparsec), strong evolution of the luminosity functions, and broad-band emission covering the entire electromagnetic spectrum (see [13] Padovani et al., 2017). The latter property means that AGNs have been observed at all wavelengths. This is partly responsible for the very large number of classes and sub-classes used in literature to describe AGNs, together with the strong dependence on the wavelength and the line of sight of the observer with respect to the AGN itself. Different methods are employed in different bands to identify these sources but, most importantly, the various wavelength regimes provide different windows on AGN physics. Namely, the infrared (IR) band is mostly sensitive to obscuring material and dust, the optical/UV band is related to emission from the accretion disk, while the X-ray band traces the emission of a (putative) corona. γ-ray and high flux density radio samples, on the other hand, preferentially select AGN emitting strong non-thermal (jet related) radiation.

Particularly important for this work is the Spectral Energy Distribution (SED) of blazars (see 1.3), that is the flux density as a function of energy and is generally characterized by two emission peaks at low and high energies (HE; E > 100 MeV) respectively, the first located at IR/optical frequencies (in several cases reaching the UV/X-ray band), and the second in the X-ray to γ-ray energy band. The physical process that is believed to produce the low energy peak is synchrotron emission from relativistic electrons in the jet, while inverse Compton scattering is thought to be at the origin of the higher energy peak, but it is not clearly understood and different models have been proposed depending on the specific blazar.

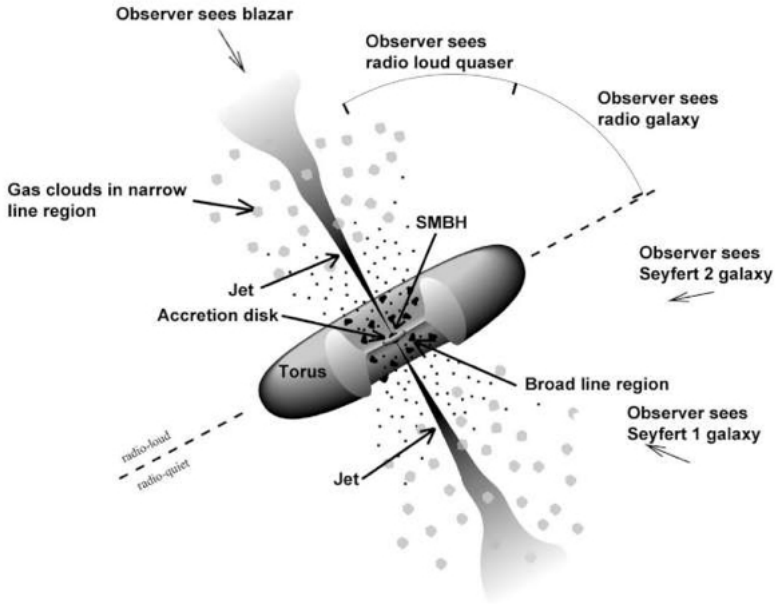

Figure 1.1: AGN scheme for the unified model.

1.3 AGN's classification

The model we have introduced can describe a vast number of apparently different objects and their different behaviour strongly depends on the observational perspective, as a consequence the classification of active galactic nuclei tends to be very vast and different depending on the specific characteristic being considered. We can identify a first classification of AGNs due to their optical-UV or radio properties and in particular we can divide AGNs according to whether the FWHM of the optical-UV emission lines are greater or not than 2000 km s^{-1}, that allows to define three main families

- **Type 1 AGN** are characterized by a strong continuous component and show bright and large Doppler-broadened emission lines, produced by high-velocity hot gas. Within this class we can identify two groups: it is possible to observe sources that have a strong emission in the radio frequencies (`radio-loud` AGN), but also non active sources that emit in this frequencies (`radio-quiet` AGN). The sources of the first group which present low luminosity are called `Broad-Line Radio Galaxies` (BLGR), the ones that are characterized by a strong luminosity are called `radio-loud quasars`. We can recognize a further division of the latter group into two subgroups due to the radio spectrum shape: we have the `Flat Spectrum Radio quasar` (FSQR) and the `Steep Spectrum Radio quasar` (SSQR). The second class of sources (radio-quiet) includes low-luminosity `Seyfert 1` and the higher luminosity `radio-quiet quasars` (QSO) .
- **Type 2 AGN** are, instead, characterized by a weaker continuous component and narrow emission lines, indicating the absence of massive gas outflows or, more likely, the presence of the dust-gas torus that covers. The radio-quiet group includes `Type 2 Seyfert` galaxies and the narrow-emission-line X-ray galaxies characterized by a general low luminosity, the radio-loud group is instead composed by Narrow-Line Radio Galaxies (NLRG) that can be distinguished on the basis of the spectrum in `Type 1 Fanaroff-Riley` (FR I) and `Type 2 Fanaroff-Riley` (FR II) galaxies.
- **Type 0 AGN** is a little group of AGNs that has specific and singular characteristics that are not described by the previous definitions: their jets are orientated very close to the observer's line of sight, they lack strong emission or absorption lines and have have a strong continuum and variable spectra, we find among this class the `BL Lacertae` objects (BL lacs) that are radio-loud AGNs and the `Broad Absorption Line` (BAL) quasar that are, instead, radio-quiet AGNs.

Blazars are generally classified in two groups namely `Flat Spectrum Radio Quasars` (FSRQs) and `BL Lacertae` objects (BL Lacs) on the basis of their optical emission/absorption line features (Urry&Padovani, 1995 [15]). FSRQs are observed to exhibit typical quasar-like optical spectra with strong and broad spectral

lines whereas BL Lacs have mainly featureless optical spectra with weak/narrow or no spectral lines. We have to underline that there's a small group of Type 1 quasars that have an emission spectrum that is really similar to the one of the BL Lacs and altogether they are identified as **blazars**.
Historically, blazars host the most energetic phenomena, thanks to the alignment between the object's axis and the observer's line of sight, and although they represent only several per cent of the overall AGN population they largely dominate the high-energy extra-galactic sky. According to the classification described above, blazars include both Type 1 FSQRs ant Type 0 BL Lacs. All blazars show the characteristic signatures of beamed emission from the central core along the line of sight: e.g. broad-band non-thermal spectrum, strong variability in time as well as in spectrum, and apparent superluminal motion.

For most of the blazars, the observed γ-ray emission is ascribed to the leptonic models in which inverse Compton (IC) scattering of the low energy photons by the relativistic electrons in the jet results in the production of the highest energy γ-ray photons. The so called synchrotron self-Compton (SSC) model is the simplest scenario to explain the γ-ray emission mostly from the BL Lac type of blazars through the IC scattering of low energy synchrotron photons by the same population of relativistic electrons that produce synchrotron photons in the jet. If the soft target photons for the IC scattering originate from regions outside the jet, the process is referred to as external Compton (EC) and this model is generally invoked to explain the γ-ray emission from the FSRQ type of blazars If the soft target photons for the IC scattering originate from regions outside the jet, the process is referred to as external Compton (EC) and this model is generally invoked to explain the γ-ray emission from the FSRQ type of blazars. Time dependent one zone SSC models have also been proposed to explain the flaring activity of a few selected blazars Alternatively, hadronic models are invoked to describe the HE γ-ray emission from a few blazars through the synchrotron radiation of ultra-relativistic protons in the jet magnetic field or through the photo-pion production followed by pion decay. However, a complete understanding of the γ–ray emission from blazars remains to be ascertained in high energy astrophysics.

1.4 1ES 1218+304

The source we have considered is 1ES 1218+304 (*Fermi* catalog name: 4FGL J1221.3+3010) and belongs to the group of blazars that exhibit hard γ-ray spectrum from the MeV/GeV to TeV band. The source shows clear variability both in the LAT energy band and in the Cherenkov band. The source first appeared in the catalogue of 3235 radio sources observed at 408 MHz with the Bologna Northern Cross telescope (B2 survey) in 1970 , with a measured redshift of z=0.182. On the basis of following observations in radio, optical and X-ray energy bands, 1ES 1218+304 was predicted to be a TeV BL Lac candidate. The MAGIC telescope discovered the first VHE γ-ray signal from 1ES 1218+304 with a 6.4σ significance above an energy threshold of $\sim$ 0.12 TeV in 2005 ([5]).

Among other successive observations a significant one was related to the VERITAS telescopes that detected VHE γ-ray emission from 1ES 1218+304 with a statistical significance of 10.4σ in 2007 confirming the discovery by the MAGIC collaboration (Acciari et al., 2009 [4]). The first evidence for the variability in VHE γ-ray emission from the blazar 1ES 1218+304 was detected by the VERITAS telescope during the high activity of the source in 2009 (Acciari et al., 2010 [3]).
The Fermi-LAT (Large Area Telescope) is continuously monitoring the HE γ-ray emission from 1ES 1218+304 and has reported this source as one of hardest spectrum blazar above 0.1 GeV in its successive catalogs.

Chapter 2

The Large Area Telescope (LAT)

The *Gamma-ray Large Area Space Telescope* (GLAST), then renamed the *Fermi Gamma-ray Space Telescope*, launched June 11, 2008, is the result of an international collaboration, which involves space agencies and research institutes in the United States, France, Germany, Italy, Sweden and Japan, and represents a state-of-the-art instrument for studying high energy astrophysics.

Fermi Gamma-ray Space Telescope monitors all regions of the sky every 3 hours and carries two main instruments: the Large Area Telescope (LAT), which is GLAST's primary instrument and the GLAST Burst Monitor (GBM), a complementary one. The GBM detects X rays and γ rays in the energy range between 8 keV to 30Mev. It consists of 12 scintillation detectors made of Sodium Iodide doped with Tallium NaI(Tl), for the lower part of the energy range, and 2 Bismuth Germanate (BGO) scintillation detectors for the high-energy range, where it overlaps with the LAT's lower-energy limit. The detector is designed for the observation of the GRBs (γ-ray bursts); for bursts over a established threshold the Fermi telescope is automatically re-pointed in this way it enables the observation of the phenomenon for the following 5 hours.
The LAT covers an energy range of $\sim$20 MeV to $\sim$300 GeV and it is composed of a tracker, a calorimeter, an anti-coincidente detector (ACD) and a system for the trigger and data acquisition and a readout system managing the trigger, data acquisition, event filtering and downlink. Moreover the high energy limit of the LAT overlaps with the energy range in which work the ground based Cherenkov Telescopes like MAGIC, VERITAS, H.E.S.S. and CTA. ref[] The LAT is described in detail in the next sections.

Parameter	Value/Range
Energy Range	20 MeV – 300 GeV
Peak Effective Area	$> 8000\ cm^2$
Energy Resolution (eq. Gaussian 1σ ; on-axis)	$< 10\%$
Single photon Angular Resolution (space angle):	
>10 GeV	$< 0.15°$
100MeV	$< 3.5°$
Single Event Readout Time (dead time)	$< 100\ \mu s$
Source Location Determination	< 0.5'

Table 2.1: Specifications of the Fermi LAT available at [7].

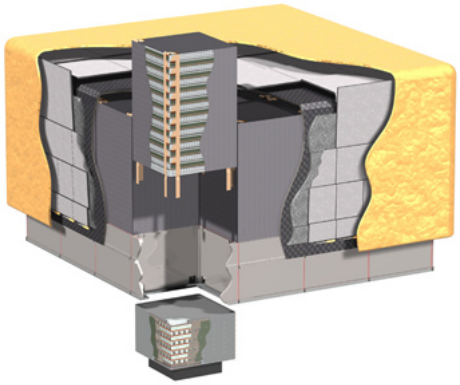

Figure 2.1: .
View of the Fermi LAT instrument with the Anti-Coincidence Detector "opened" in yellow, and the tracker and calorimeter part of one tower separated for more clarity.

2.1 The tracker

A high energy γ-ray cannot be reflected or refracted, and interacts with matter mainly through pair production (usually e^+ e^- production). Thus, the aim of the tracker is to reveal the electron's and positron's trace with high efficiency and resolution. The LAT Tracker consists of a four-by-four array of tower modules: each tower module consists of x-y layers of Silicon-Strip particle tracking Detectors (SSDs) interleaved with thin, high-Z (Tungsten) foils to increase the probability of conversion. A γ-ray passes through the thin anti-coincidence detector without interacting and advances in the tracker. If it interacts, typically in a conversion foil, it produces an electron-positron pair, that, interacting with matter, undergo ionization, depositing energy in the volume of the SSDs and a signal is produced in the electronics. The pair conversion topological signature in the tracker is also used to help reject the much larger background of cosmic rays. An esteem of the deposited energy is obtained.

2.2 The calorimeter

The Calorimeter causes an electromagnetic shower and measures the energy of the event. The LAT Calorimeter is made of an arrangement of Cesium Iodide crystals with the same four-by-four array structure of the tracker. In the scintillator crystals ionization is converted into flashes of light, the light is collected by Silicon photodiodes and converted into an electrical signal which is read out by the Calorimeter electronics. The light signal is proportional to the fraction of the absorbed energy, and the value can be corrected for the amount lost due to the finite size and due to the gaps.
The Calorimeter also helps to reject cosmic rays, since their pattern of energy deposition is different from that of γ rays.

2.3 The Anticoincidence Detector (ACD)

The ACD has the purpose to discriminate charged particles and plays a crucial role in the charged background rejection: indeed one of the major problems within the γ detection is represented by the background cosmic rays that strike the detector in great amounts.

Having a very high efficiency in detecting when a single charged particle enters the field of view of the telescope is fundamental (of at least 3000:1). The ACD is made of plastic scintillators, the light is collected from each tile by the Wavelenght Shifting Fibres and re-emetted at a higher wavelenght, thus guaranteeing a better coupling between the scintillator and the photomultiplier, which are located around the lower perimeter of the ACD.
The high efficiency is linked to the "backsplash" phenomenon: secondary particles isotropically distributed and generated by the electromagnetic shower in the Calorimeter can produce a signal in the ACD via Compton effect, comparable to that of a minimum ionizing particle and it could be mistaken to be a charged particle. The entire would then be rejected. To prevent this self veto effect the ACD is segmented, and the location of the veto in the ACD can be correlated to the signals in the other detectors.

2.4 Data Acquisition and Trigger

The Data Acquisition Sistem (DAQ) has the role of collecting and processing the data from the other subsystems. The DAQ manages the hardware trigger, performs a single event reconstruction, and applies the on-board filter, before sending the events' data for downlink. The instrumental dead time is associated with the time needed to read out the LAT detectors: the programmable trigger system is optimized to start the read out only for interesting events, notably γ-ray candidates. The on-board filter ensures a good use of the available bandwidth, maximizing the fraction of "good" events and rejecting clear background events. When an event reaches the data pipeline on ground a more complex event reconstruction is

performed, and a very effective background rejection is performed, trained on the Monte Carlo simulation of the detector.

2.5 Fermi LAT Performance

The LAT performance is governed primarily by three factors:

- LAT hardware design
- event reconstruction algorithms
- background selections and event quality selections

A result of the performance analysis is the production of full Instrument Response Functions (IRFs), describing the performance of the instrument as a function of photon energy, incidence angle, conversion point within the instrument, and other important parameters. An IRF is the mapping between the incoming photon flux and the detected events, and depends not only on the LAT hardware but also on the processing that calculates the event parameters from the observables and assigns probabilities that an event is a photon.
The IRF is factored into three terms:

– *efficiency* in terms of the detector's effective area; i.e. the efficiency multiplied for the geometrical area of the detector;

– *resolution* as given by the Point-Spread Function (PSF), i.e. the probability density that a photon with a defined energy E_0 and direction $\hat{p_0}$ is detected with direction $\hat{p}$;

– *energy dispersion*, the probability density that a photon with a defined energy E_0 and direction $\hat{p_0}$ is detected with energy E

Each event class is defined by event selection cuts and has a corresponding set of response functions that are unique to that class. The response functions for each class are internally partitioned into FRONT and BACK conversion types.

In Figure (2.2) we show the plot relative to the effective area and in Figure (2.3) the one relative to the the Point Spread Function.

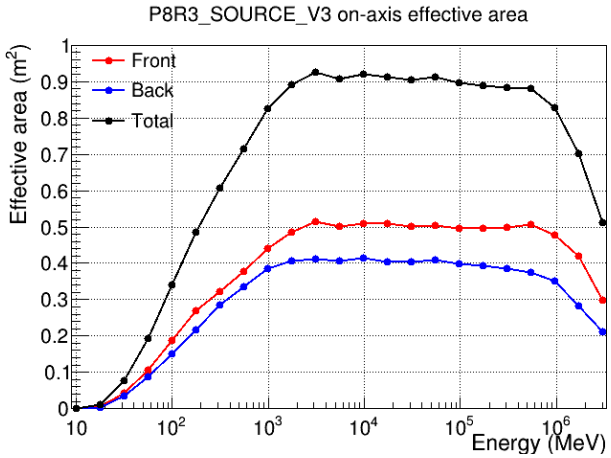

Figure 2.2: the effective area as a function of energy for normal incidence photons (θ=0) shown down to 10 MeV.

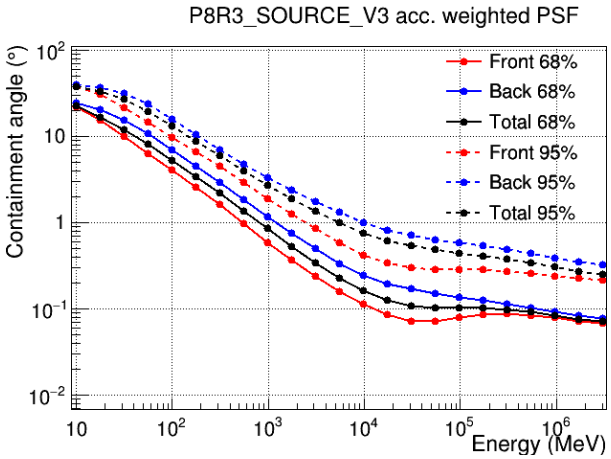

Figure 2.3: 68% and 95% containment angles of the acceptance weighted (acc. weighted) PSF for both the front/back and PSF event types.

Chapter 3

Analysis Methods

The official analysis method of the Fermi collaboration to date is the *Maximum Likelihood Analysis*. This analysis approach, described in the following section, is applied to photon counts and is used to estimate to what extent the observed data are consistent with a statistical hypothesis.

3.1 The Likelihood Analysis

To derive information from the measured events, e.g. the flux or spectral index of a source, we use the maximum likelihood method, which estimates the values of the set of parameters maximizing the likelihood that the chosen source model fits the collected data, thus identifying the set of parameters that better represent our data. Specifically, the analysis refers to a model that describes the distribution of the γ sources including their intensity, morphology and spectral properties in the sky: it is obtained considering all the known point sources and the two diffuse background sources, namely the Galactic diffuse component and isotropic extragalactic component, which will be discussed in Section (3.3). Each source model is described by a set of attributes, and for each a range of valid values can be specified. During the analysis, parameters can be fixed (freezed) and freed (thawed) according to the results. The best set of parameters with the given constraints is evaluated by minimizing `-log(likelihood)`. A good starting point for all parameters is given by the public Fermi LAT source catalog, that includes fit parameters for all sources for a time selection of 12 years (in the current release, 4FGL-DR3 [2]).“

In addition, the likelihood methods allow to solve different problems, such as the detection of weak sources, localization of point sources and to evaluate uncertainties. In particular, for the detection of point sources a specific quantity called Test Statistic (TS) can be defined [12]. A tentative source is added to the model, with only the number of event counts as a free parameter, the TS is the improvement in likelihood and behaves as a χ^2 distribution with 1 degree of freedom, thus its square root can be approximately assumed as the number of Gaussian *sigma*s associated with the detection.

3.2 The Unbinned Analysis

Two types of analyses can be performed with the Fermi analysis software: binned and unbinned, the latter being the preferred method for time series analysis of the LAT data. Formally, the unbinned analysis is obtained when the binning is small enough that the number of events in each bin is one or zero. The drawback is obviously the computational cost. We choose the unbinned analysis because we are working with a point source at high energies, so we expect the event count to be small, of the order of 10.000 photons. The details of the unbinned analysis will be better discussed in Section (4.1).

3.3 Diffuse γ-ray emission

An important ingredient for the likelihood analysis is the model which describes all the radiation emitted in the selected ROI. A fundamental first step is to provide an accurate description of the diffuse emission in the interstellar space, constituting almost 80% of the events in the LAT dataset. We can identify two main components of the diffuse emission: the Galactic *diffuse* emission and the *isotropic* component.
Continuum diffuse γ-ray emission (DGE) is produced in our Galaxy (mainly in the Galactic plane) by interactions of high-energy cosmic rays (CRs) with interstellar matter and low-energy radiation fields. A weaker diffuse component is observed with almost isotropic distribution all over the sky, and it is thought to be extra-Galactic in origin. This emission is usually referred to as the extra-Galactic gamma-ray background (EGB). The great majority of the EGB can be attributed to unresolved populations of extra-Galactic gamma-ray point sources, primarily the nuclei of active galaxies including blazars. In addition, the isotropic component includes the instrumental backgrounds: charged particles misidentified as photons and true photons created in the LAT materials by incoming CRs ("irreducible background"). The LAT Collaboration develops and distributes models for the two diffuse components, to be included in the source models for the likelihood analysis. From what we have discussed, the isotropic emission varies depending on the event class, since the residual background varies, while the Galactic emission is not affected, being a proper γ-ray source.

Chapter 4

Analysis of 1ES 1218+304

As we said in Section (1.4), the source 1ES 1218+304 (Fermi catalog name: 4FGL J1221.3+3010) belongs to the group of blazars that exhibit hard γ-ray spectrum from the MeV/GeV to TeV band. The source shows clear variability both in the LAT energy band and in the Cherenkov band, this variability can be observed in the light curve that is obtainable from the Fermi LAT Light Curve Repository [11] and is shown in Figure (4.1). Clearly there is a strong variability during the whole data taking period of the Fermi LAT.

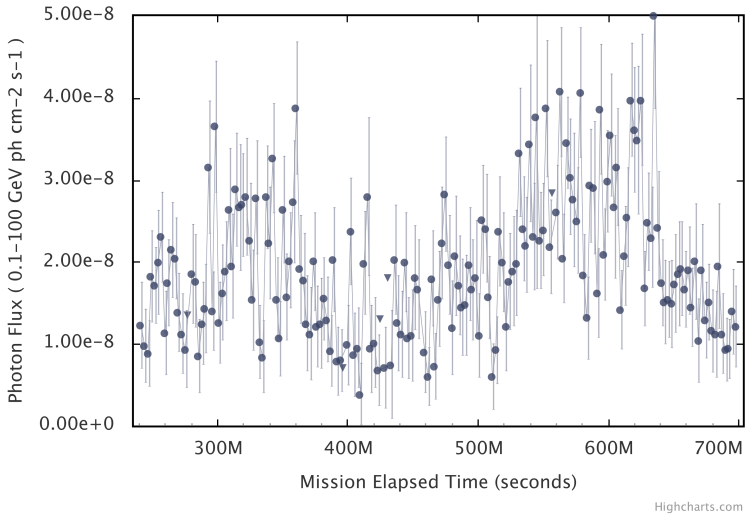

Figure 4.1: Monthly light Curve of 1ES 1218+302 from the Light Curve Repository.

The analysis consists of the following parts.

- Fit of the LAT high energy band (E > 5 GeV). The catalog provides a broken power law model for the source (corresponding to a parabola in log-log scale), but we are going to verify that for our selection a simple power law is enough (a line in log-log scale) because we are working at energies beyond the expected blazar's peak

- Evaluation of the variability of the spectral shape (e.g. spectral index for a power law) with the source intensity, comparing the spectra at low, medium and high flux.
- Comparison with Cherenkov data taken during flaring activity. This will allow us to introduce corrections due to Extra-Galactic Background Light

4.1 Fermi LAT Data Extraction

For the analysis of 1ES1218+304 we follow the standard procedure recommended by the LAT collaboration [6]. In the current analysis γ-ray data from the observation of **1ES 1218+304** from October 2010 to October 2022 were obtained from the data portal and analyzed using the standard analysis procedure provided by the Fermi-LAT collaboration. The data can be found on the website and can be freely downloaded in *FITS* format (Flexible Image Transport System), frequently used in astronomy.

Before extracting the data we have to define the region of interest (ROI) in the sky, because we want to study a very specific source, and after that we also need to select the time and energy ranges. For the time data we have used the Mission Elapsed Time (MET) time system that measures time in seconds starting from January 1 2001.
The events where selected in the energy range from 5 GeV to 300 GeV, within a circular region of radius 10° centered on the position of 1ES 1218+304 obtained from the Fermi LAT 12-Year Point Source Catalog. Such a ROI is suitable for a point source, as it is larger than the 68 % containment angle of the PSF at lowest energies ($\sim 3^{\circ}$), see Figure (2.3). This ensures that most photons coming from the source to be detected are included, and limits the amount of unnecessary data.

We used the `P8R2_SOURCE_V6` instrument response functions, matching our class selection. A zenith angle cut of 90° was applied to reduce the contamination due to the γ-rays from the bright Earth's limb (located at a zenith angle of 113°).

RA	$12^{\circ}\,21'\,22.8$”
DEC	$+30^{\circ}\,10'\,0.4$”
Search radius	10°
Observation Dates (s)	Δt= 309582233 - 688273433
Energy Range (GeV)	ΔE = 5 - 300

Table 4.1: Data selection inputs.

4.2 Likelihood Analysis with Python

The previous selections allow to perform the likelihood analysis with Python. Data were analyzed using Fermi ScienceTools v1.2.1.
The model file containing the spectral parameters of all known γ-ray emitting sources located within the ROI was generated including all the sources in the fourth Fermi-LAT source catalog of γ-ray sources (4FGL) [2] (using the publicly available `make4FGLxml.py` script). Sources just outside the ROI are included since they still produce counts inside. The Galactic and extra-Galactic diffuse γ-ray emission were parametrized using `gll_iem_v07` and `iso_P8R3_SOURCE_V2_v1` models. The parameters of all sources within the ROI, as well as the normalization of diffuse components, were left free to vary during the initial fitting, while the spectral parameters of sources outside the ROI were fixed to their catalog values. We checked the values obtained from this first fit, in particular checking the test statistic (TS) values for all point sources in the model. We removed all the sources that had small TS values (< 4) to simplify the model and speed up the analysis (mostly soft sources).

We ran the analysis again, to obtain a second evaluation of the spectral parameters together with their errors. We evaluated how the normalization of the galactic and isotropic components relate to the default values, finding:

$$flux_{gal} = (1.2 \pm 0.1)\ cm^{-2}\, s^{-2}\, MeV^{-1}$$
$$flux_{iso} = (1.02 \pm 0.06)\ cm^{-2}\, s^{-2}\, MeV^{-1}$$

Both are compatible with 1, thus we fixed the flux to the default values. We will verify this again for the low-medium-high flux selections. Mind that, while the correlation with the point source is small, due to the different spatial distribution, the correlation between Galactic and isotropic is large since we are close to the Galactic North Pole (`Gal b` $= 82.7°$ at the ROI center, see Figure (4.2)) and the Galactic component has very little spatial features.
For the source the differential flux is described in the catalog by a Log Parabola model that has the following expression:

$$F(E) = \frac{dN}{dE} = F_0 \left(\frac{E}{E_0}\right)^{-(\alpha + \beta log(E/E_b))}$$

for which we fitted the parameters reported in Table (4.2).

F_0 $(cm^{-2}\, s^{-1}\, MeV^{-1})$	α	β	E_0 (MeV)
$(1.4 \pm 0.7) \cdot 10^{-12}$	3.0 ± 0.5	-0.02 ± 0.01	2759

Table 4.2: Values of the parameters obtained for the LogParabola model.

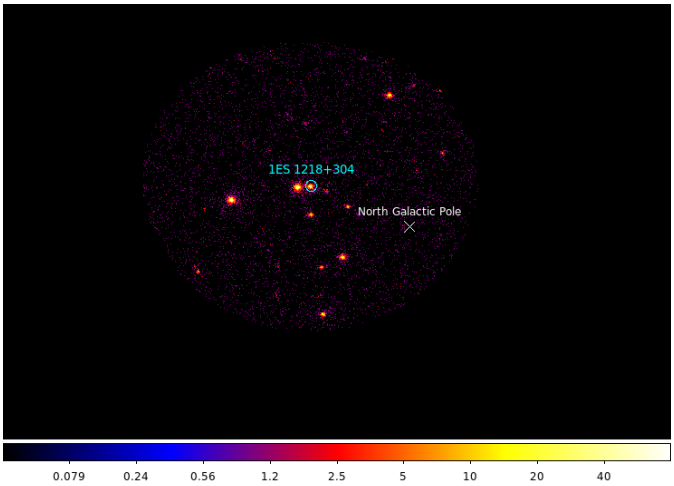

Figure 4.2: Counts map of the selected ROI.

We are working in the energy range between 5 GeV and 300 GeV, an interval in which we expect the differential spectrum of the source to be beyond its peak: this is reflected by the parameters of the fit where β can be fixed to 0, transforming the model into a Power Law, with the following expression:

$$F(E) = \frac{dN}{dE} = F_0 \left(\frac{E}{E_0}\right)^{-\Gamma}$$

where F_0 is the flux normalization at energy E_0 and Γ is the observed photon spectral index.

We modify the model accordingly, change the source description and we fit our sample again, this time performing also an evaluation of the flux as a function of energy (with the the `likeSED.py` user contributed tool). Data are divided in energy bins, and a likelihood fit is ran in each of these individual bins; the resulting fluxes give the flux points shown in the next figures.

To minimize the effects of the correlation among the model parameters we also set the scale energy E_0 to the *decorrelation value*. Evaluating the relative uncertainty on the flux one finds, for a Power Law model:

$$\frac{\Delta F^2}{F^2} = \left(\frac{\Delta F_0}{F_0}\right)^2 + ln^2\left(\frac{\Delta E}{E_0}\right)\Delta\Gamma^2 - \frac{2}{F_0}\, cov(F_0, \Gamma)\, ln\left(\frac{E}{E_0}\right)$$

as defined in [1]. where $cov(F_0, \Gamma)$ is the covariance term returned by the `NEW MINUIT` minimization and error analysis function called by the Fermi likelihood analysis tool `gtlike`, while ΔF, ΔF_0 and $\Delta\Gamma$ are the statistical uncertainties on the flux F, the prefactor F_0 and the index Γ at energy E. The relative error of the flux reaches a minimum at the decorrelation energy E_{dec}, defined as

$$E_{dec} = E_0\, exp\left(\frac{cov(F_0, \Gamma)}{F_0\, \Delta\Gamma^2}\right)$$

where the contribution of the uncertainties on Γ vanishes. We evaluated E_{dec}, changed the parameter in the model and fitted again. We obtained $E_{dec} = 13087$ MeV, which gives the final fit parameters reported in Table (4.3) for the **PowerLaw** model.

Prefactor	$(3.53 \pm 0.2) \cdot 10^{-14}\ cm^{-2}\ s^{-1}$
Index	-1.80 ± 0.04
Scale	13087 MeV
Flux	$(1.20 \pm 0.05) \cdot 10^{-9}\ cm^{-2}\ s^{-1}$

Table 4.3: Fit parameters using a PowerLaw model for the source with minimal correlation, including the integrated flux in our range.

The values of the uncertainty, as calculated above, allow us to perform the so called butterfly plot, or bow-tie plot: we can plot the spectrum, with the 1σ uncertainty as a function of energy shown as a band around the fit, as seen in Figure (4.3).

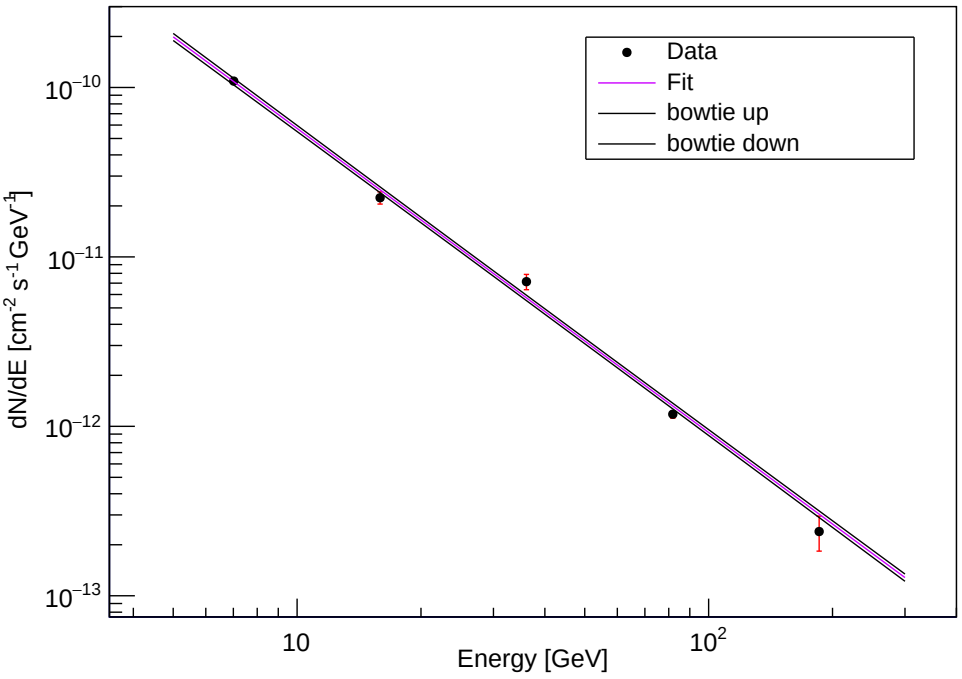

Figure 4.3: Bowtie plot in log-log scale for the 12 year sample.

4.3 Source Variability

In this section we study the spectral parameters as a function of the source level of emission, as evaluated from the monthly light curve in Figure (4.1).

The variability of blazars can be very strong and the SED can undergo significant changes during the whole observation. The parameters we estimated in the first part represent just the average values in the whole period, so it becomes necessary to analyze smaller subsets to verify if the source spectrum changes.
Using the monthly light curve we proceed as follows. First we created an histogram of the monthly flux values, in Figure (4.2). Then we evaluate two percentiles, dividing the histogram in three parts cutting at 50% and 83% of the area. Thus, in the first set we have 50%=3/6 of the times, when the source is in a low status. In the second selection we have 2/6 of the times, when the source is in an intermediate state. In the final set we have 1/3 of the times, when the source is in a high state. The percentiles were chosen so that, at order zero, the expected number of counts from the source in the three data sets would be comparable. In Figure (4.4) the division in the three sets is shown.

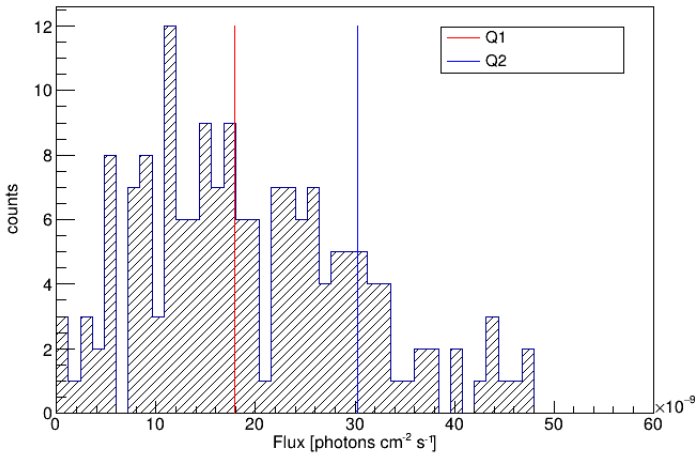

Figure 4.4: Flux counts histogram based on Fig (4.1)

For each class (low, medium, high) we created the corresponding datasets performing the necessary time selections, then we repeated the analysis excactly as described in the previous section.

First we consider the normalization of the Galactic and isotropic diffuse components for each of the three flux classes, which are shown in Table (4.4). For each class they are reasonably compatible with the default value of 1, so we fixed their values to that as we did for the total sample.
From the likelihood fit we obtain the final values of the parameters for each class which are shown in Table (4.5).

The values of the photon index Γ do not show particular variations, this is confirmed by their compatibility within the errors. The index for the Low subset indicates a possible softening of the spectrum with respect to the remaining two,

Component	differential flux $(cm^{-2}\,s^{-2}\,MeV^{-1})$		
	Low	Mid	High
galactic	(1.03 ± 0.06)	(1.15 ± 0.01)	(0.93 ± 0.03)
isotropic	(0.90 ± 0.03)	(0.892 ± 0.006)	(0.91 ± 0.02)

Table 4.4: High, mid and low values of galactic and isotropic components.

Component	Flux $(cm^{-2}\,s^{-1})$	Γ	Prefactor F_0 $(cm^{-2}\,s^{-1})$	Scale E_0 MeV
Low	$(6.8 \pm 0.6) \cdot 10^{-10}$	-1.90 ± 0.09	$(2.4 \pm 0.2) \times 10^{-14}$	11920
Mid	$(1.30 \pm 0.09) \cdot 10^{-9}$	-1.76 ± 0.07	$(3.8 \pm 0.2) \times 10^{-14}$	13210
High	$(1.8 \pm 0.1) \cdot 10^{-9}$	-1.74 ± 0.08	$(3.6 \pm 0.3) \times 10^{-14}$	15990

Table 4.5: Fit parameters for high, mid and low subsets.

but it is not significant. On the other hand, this goes in the expected direction, with hardened spectrum during active periods.

The spectra are compared in Figure (4.5); the curve for the whole data set has been added for completeness, and it lies close to the medium one as could be expected. We also plotted bowtie uncertainties bands and SED data points for each class, in Figure (4.6). The width of the 68% confidence band is more evident than in Figure (4.3), due to the lower statistics.

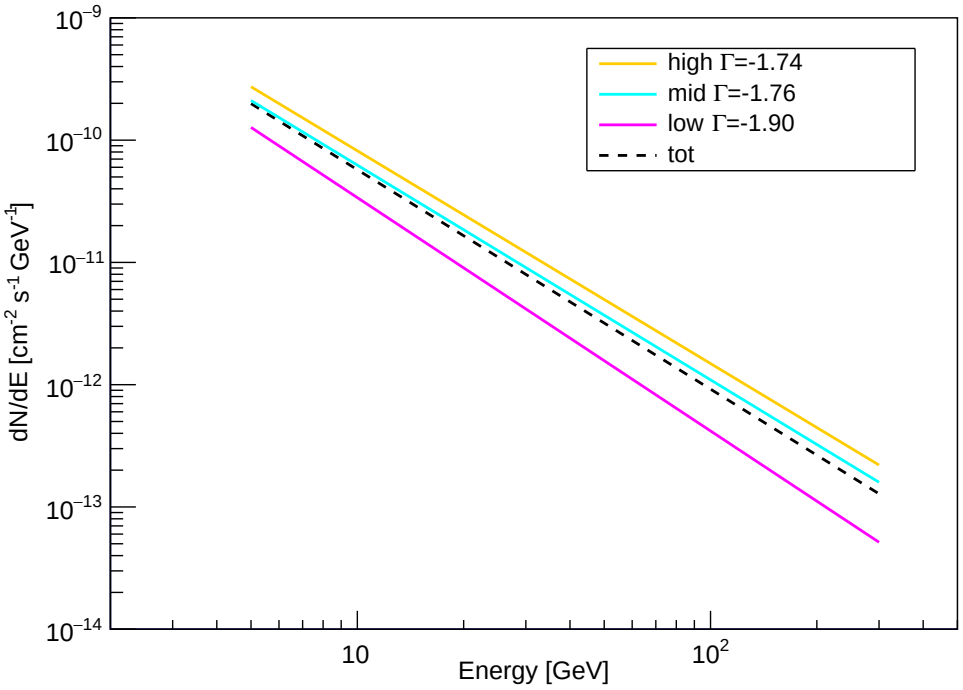

Figure 4.5: Comparison of high, medium, low with total (average) Power Law fit.

Figure 4.6: Bowtie plot for each class.

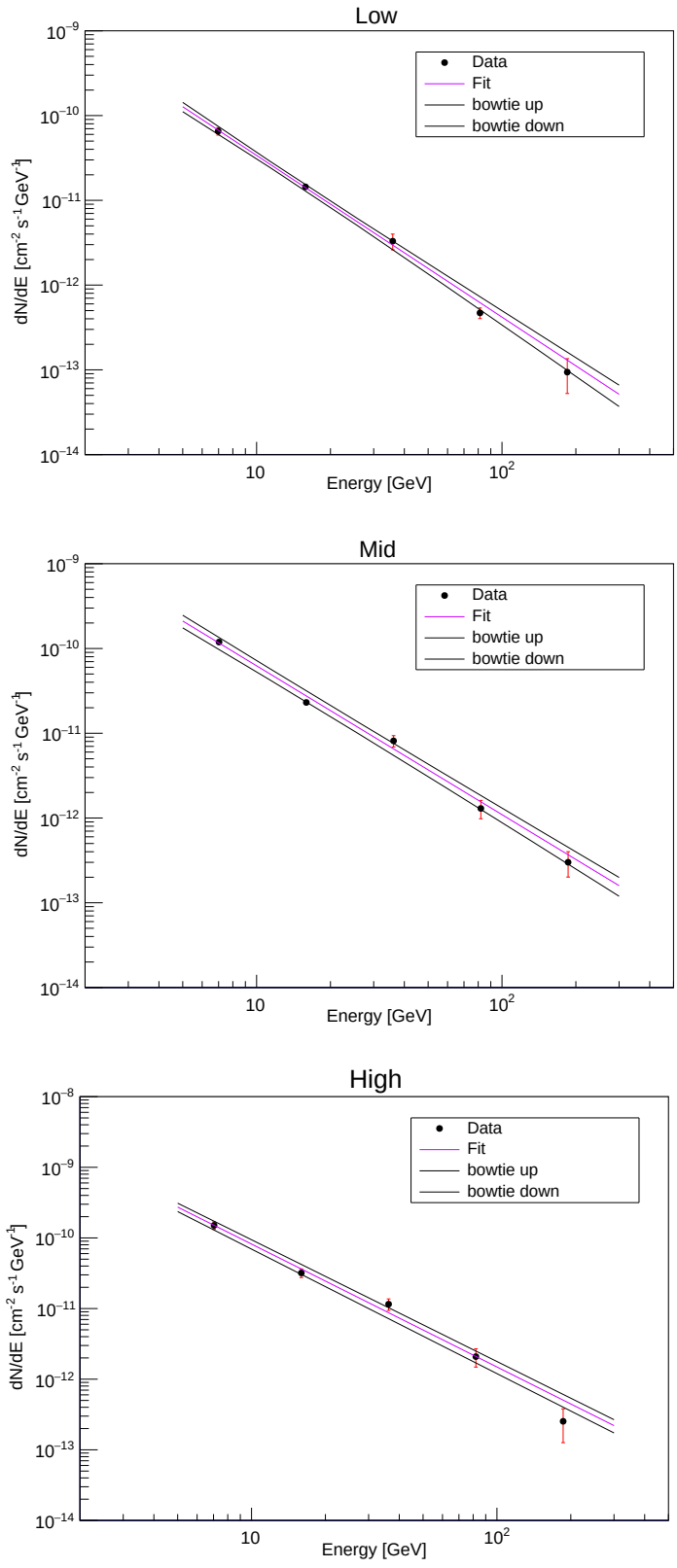

4.4 Cherenkov Data Comparison

In the VHE band, statistically significant detections of γ-ray photons from 1ES 1218+304 at two occasions [14] have been reported by VERITAS ground based Cherenkov telescope. The observed differential VHE γ-ray spectra is well described by a power law of the form we have described before in Section (4.2). The spectral indexes derived from the VHE γ-ray observations of 1ES 1218+304 at different epochs from VERITAS are summarized in Table (4.6).

Year	Energy Range TeV	Γ	Reference
2007	0.16-1.8	3.08 ± 0.34	VERITAS (Acciari et al. 2009)
2009	0.16-1.8	3.07 ± 0.09	VERITAS (Acciari et al. 2010)

Table 4.6: VHE γ-ray observations from the blazar 1ES 1218+304 between 2005 and 2018.

It is evident from the values of the index $\Gamma \sim 3.0$ that the observed VHE γ-ray spectra of the blazar 1ES 1218+304 at two epochs is softer than the HE spectrum measured from the Fermi-LAT, as can be seen in the spectral comparison in Figure (4.7). The softening of the observed VHE spectra can be attributed to the absorption of TeV photons by the low energy Extra-Galactic Background Light (EBL) due to the high redshift (z = 0.182) of the source, and will be addressed in the next section.

The VHE γ-ray emissions in the low activity state of this source detected by VERITAS telescopes are observed to suffer a large attenuation due to EBL absorption, so the intrinsic VHE emission could in reality be consistent with the photon spectral index of ≤ 2 we have found. We are going to verify this in the next section.

4.5 EBL corrections

TeV γ-ray photons are suppressed by interaction with the IR/optical low-energy photons of the EBL via $e^- e^+$ pair production while propagating from source to the observer [10], leading to a cutoff in the measured γ-ray spectrum. The optical depth τ of the attenuation is a complex function of the γ-ray photon energy, the distance to the source (z), and the cross-section for pair production, and it is related to the density and spectral energy distribution of the cosmic background radiation along the line of sight. For a given source, the observed γ-ray flux F_{obs} is related to the emitted flux F_{emi} by the following relation

$$F_{obs} = F_{emi}\, e^{-\tau(E,z)}$$

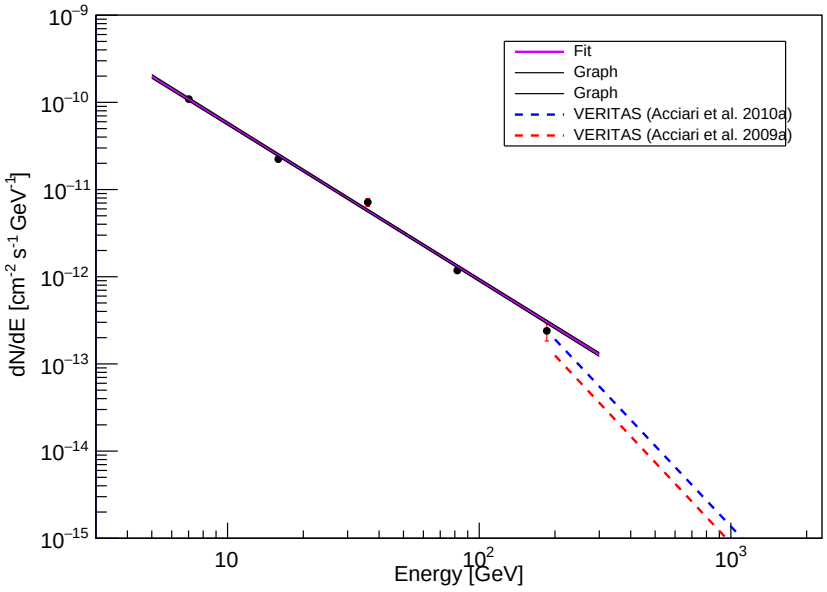

Figure 4.7: Comparison of VERITAS observations with our spectrum from Figure (4.3).

For a proper comparison of the GeV and TeV spectra is therefore necessary to correct for the EBL attenuation and estimate the intrinsic spectrum of 1ES 1218+304. Conversely, this provides a way of probing the EBL with TeV γ-ray observations. Since the EBL, from the IR through the optical and into the UV, is the total light from all of the stars that have ever existed in the Universe, knowledge of the EBL is important for understanding the evolution of our Universe and the formation of stars and galaxies. Bright foreground sources from the Milky Way and Solar System make direct measurements of the EBL challenging.

In particular EBL is a fundamental source of opacity for cosmic high energy photons, because it suppresses most of the flux of distant γ-ray sources, as well as a limitation for the propagation of high-energy particles in the Universe. The *cosmic γ-ray horizon* refers to that distance at which only $\sim$30% of the source flux arrives at Earth for a given energy, the detection of the highest energy photons from distant sources allows Fermi LAT measurements to probe the horizon from very low to very high redshift and has important consequences for measuring cosmological parameters, such as the expansion rate of the Universe.
In [8] determinations of the local EBL photon density in the Universe and its evolution impact on the estimate of the cosmic opacity for photon-photon interaction and pair-production, and on the HE and VHE photon horizon, has been achieved using deep survey observations by the Herschel Space Observatory and the Spitzer telescope, matched to optical and near-IR photometric and spectroscopic data, to re-estimate number counts and luminosity functions above wavelengths of a few microns, and the contribution of resolved sources to the EBL. The new data indicate slightly lower photon densities in the mid- and far-infrared and sub-millimeter

compared to previous determinations, that implies slightly lower cosmic opacity for photon-photon interactions. Applications of this improved EBL model on current data are considered, as well as perspectives for future instrumentation, the Cherenkov Telescope Array (CTA) in particular.

Using the values given in [8] for the photon-photon optical depth as a function of energy and redshift $\tau(E, z)$, we applied an EBL correction to the observed γ-ray flux. The redshift of 1ES 1218+304 (z=0.182) does not match the ones sampled in [8], so we derived the $\tau(E)$ curve by linear interpolation over z. Then we applied the correction to the VERITAS spectra.
In Figure (4.8) the Power Law from the VERITAS observations in [3] and [4] are shown before and after the EBL correction. This is only a way to give an indication of the magnitude of the phenomenon, and the curvature caused by the correction is not significant.

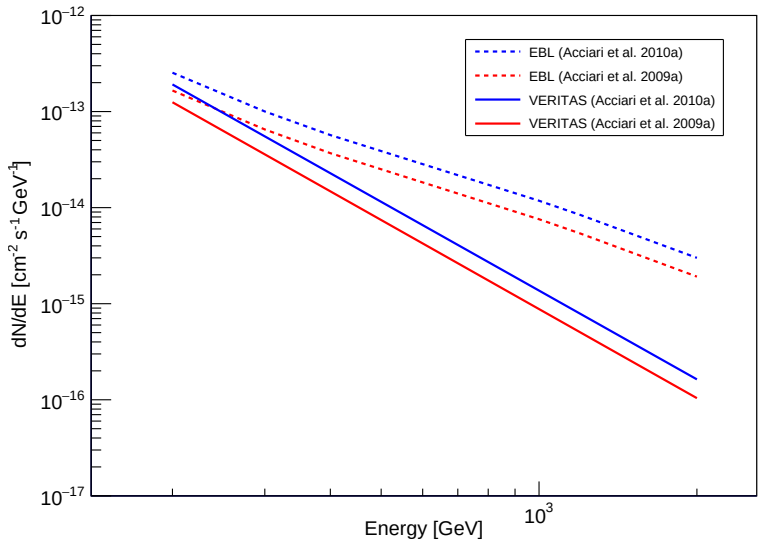

Figure 4.8: EBL correction of the results from [3] and [4]

In Figure (4.9) we compare the average LAT spectrum from Figure (4.3) (12 years, 2012-2022) with that measured by VERITAS at VHE γ-rays ($\sim$ 5 months, 2008-2009) after EBL correction. The VERITAS spectra points are corrected, including the uncertainties. A in Fig. 4.8, the spectral lines are corrected very naively as a function of E and show some curvature, while a proper fit would return a simple power law. Comparison of the spectra confirms that, to a great extent, the softening of the observed spectrum shown in Figure (4.3) can be attributed to the EBL.
Finally, we evaluate the EBL correction on Fermi analysis. Fermi software tools allow to include the EBL attenuation as a correction to the spectral fit with a PowerLaw model. The included model is [9], but we replaced the EBL data file with one we derived from [8]. We fitted our 12 years data sample with a source model that includes the EBL attenuation. We obtained from this new model an

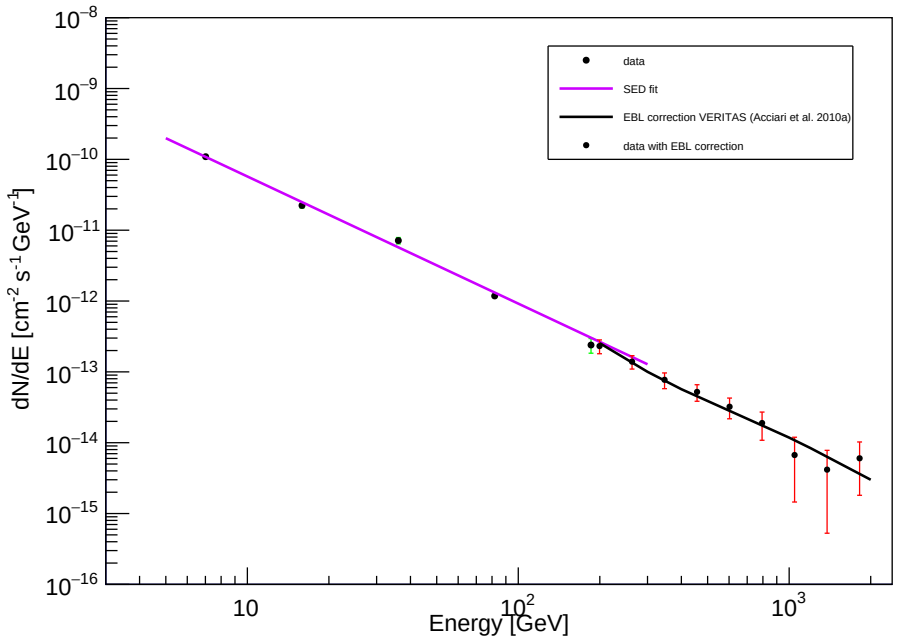

Figure 4.9: Comparison between our SED fit and EBL corrected version of [3], including experimental data points.

index value of

$$\gamma = -1.65 \pm 0.05$$

to be compared with the initial fit Γ=-1.80±0.04. The two are comparable, with a compatibility index r = 2.1 (nearly $\sim 3\sigma$). As expected the effect is much less evident in the LAT energy band.

Chapter 5

Conclusions

In this thesis we studied the HE spectral characteristics of the Active Galactic Nucleus 1ES 1218+304 using the standard likelihood method provided by Fermi Science tools: we obtained a good description of the spectrum using a Power Law model, compatible with previous observations of the source.
Then we explored the variability of the source, dividing the total sample in three classes describing the low, medium and high flux status. We observed that the spectral index does not change in a noticeable way from the total, average fit.
Finally, we compared the analysis results with the VHE observations of the source by the VERITAS collaboration, noting that they report a softening of the spectrum with respect to the LAT results. This can be explained introducing the effects of the Extra-galactic Background Light on VHE spectra. We verified the consistency between the LAT and VERITAS observations after correcting for the EBL attenuation.

Bibliography

[1] A. A. Abdo et al. “Fermi observations of the very hard gamma-ray blazar PG1553+113”. In: *The Astrophysical Journal* 708.2 (Dec. 2009), pp. 1310–1320.

[2] S. Abdollahi et al. “iFermi/i Large Area Telescope Fourth Source Catalog”. In: *The Astrophysical Journal Supplement Series* 247.1 (Mar. 2020), p. 33.

[3] V. A. Acciari et al. “Discovery of Variability in the Very High Energy γ-Ray Emission of 1ES 1218+304 with VERITAS”. In: 709.2 (Feb. 2010). DOI: 10.1088/2041-8205/709/2/L163.

[4] V. A. Acciari et al. “VERITAS Observations of the BL Lac Object 1ES 1218+304”. In: 695.2 (Apr. 2009), pp. 1370–1375. DOI: 10.1088/0004-637X/695/2/1370.

[5] J. Albert et al. “Discovery of Very High Energy Gamma Rays from 1ES 121830.4”. In: *The Astrophysical Journal* 642.2 (Apr. 2006), pp. L119–L122.

[6] *Fermi Analysis Threads*. URL: https://fermi.gsfc.nasa.gov/ssc/data/analysis/scitools/.

[7] *Fermi Instruments Specification*. URL: https://fermi.gsfc.nasa.gov/science/instruments/table1-1.html.

[8] A. Franceschini and G. Rodighiero. “The extragalactic background light revisited and the cosmic photon-photon opacity”. In: *Astronomy &amp Astrophysics* 603 (July 2017), A34.

[9] A. Franceschini, G. Rodighiero, and M. Vaccari. “Extragalactic optical-infrared background radiation, its time evolution and the cosmic photon-photon opacity”. In: *Astronomy Astrophysics* 487.3 (June 2008), pp. 837–852.

[10] R. Gould and G. Schréder. “Opacity of the Universe to High-Energy Photons”. In: *"Phys. Rev. Lett."* (1966).

[11] *Fermi LAT Light Curve Repository*. URL: https://fermi.gsfc.nasa.gov/ssc/data/access/lat/LightCurveRepository/source.html?source_name=4FGL_J1221.3+3010#.

[12] J. Mattox et al. “The likelihood analysis of EGRET data”. In: *The Astrophysical Journal* 461 (Mar. 1996), p. 396.

[13] P. Padovani et al. “Active galactic nuclei: what’s in a name?” In: *The Astronomy and Astrophysics Review* 25.1 (Aug. 2017).

[14] K K Singh et al. “Long-term multiwavelength view of the blazar 1ES 1218304”. In: *Monthly Notices of the Royal Astronomical Society* 489.4 (Sept. 2019).

[15] C. Megan Urry and P. Padovani. “Unified Schemes for Radio-Loud Active Galactic Nuclei”. In: *Publications of the Astronomical Society of the Pacific* 107 (Sept. 1995), p. 803.